A Theoretical Model of the Near Wake of a Slender Body in Supersonic Flow

JOHN T. OHRENBERGER* AND ERIC BAUM*
TRW Systems Group, Redondo Beach, Calif.

A steady-state formulation for laminar flow is employed within a region extending from the boundary layer approaching separation downstream to the axial station of the sonic point on the axis. Included are the formation of the lip shock wave, the growth of the mixing layer into the rotational inviscid wake of the boundary layer, the recirculation region, and the wake shock wave. The entire flow is treated as a viscous interaction problem. Passage of the solution through two saddle-point singularities determines uniqueness and insures that the downstream behavior is the proper one for wake flows. The flow is divided into two regions; an inner region, which includes the recirculating flow, is determined by an integral method, while an outer region employs a finite-difference technique. A rigorous matching of the flow between the two regions is included. The model is applied to a Mach 6 wedge flow corresponding to an experimental case of Batt.

Nomenclature

D = base diameter
h = static enthalpy
H = total enthalpy; also total base height
h_ψ = cross-stream metric
h_s = streamwise metric
L = body length
M = Mach number
$\dot{M}$ = mass flow
n = distance normal to streamlines
P = pressure
P_{t2} = pitot pressure
Pr = Prandtl number
r = radial coordinate
Re = Reynolds number
s = distance along streamlines
S = streamwise orthogonal coordinate
T_o = total temperature
u = axial velocity
U = total velocity
v = radial velocity
x = axial coordinate
y = lateral coordinate ($\alpha = 0$)
α = dimensionality factor (0 for two-dimensional flow, 1 for axisymmetric flow)
δ = radial coordinate of matching streamline
ζ = vorticity
θ = flow angle
λ = $1 + \alpha$
μ = viscosity
ξ = profile parameter $\rho_o u_o/\rho_\delta u_\delta$
ρ = density
σ = profile exponent
τ = shearing stress
ϕ_1 = profile parameter h_o/h_δ
ϕ_2 = profile parameter $(\delta/h_\delta)(\partial h/\partial r)_\delta$
Φ = viscous dissipation term
ψ = streamfunction and orthogonal coordinate

Subscripts

c = cone
DSL = dividing streamline
inv = inviscid
o = centerline
s = wake stagnation point
w = wedge
δ = matching streamline
∞ = freestream flow conditions

1. Introduction

THE near wake of a vehicle in supersonic flow contains a large subsonic region adjacent to the base in which the downstream flow can communicate and have an influence on the upstream flow. This zone consists of the subsonic portion of the boundary-layer prior to separation, the recirculation region up to the sonic line in the shear layer, and the subsonic flow adjacent to the axis downstream of the wake stagnation point to the axis sonic point. The mathematical treatment of this region and the adjacent supersonic flow in a steady-state formulation using the Navier-Stokes equations is a boundary value problem. However, steady-state methods based upon approximations to the Navier-Stokes equations have been applied to this and related problems in which the mathematical character of the governing equations is changed without, hopefully, significantly affecting the solution. In particular, the boundary-layer approximations change the apparent character of the equations from elliptic to parabolic. This implies that initial value methods can be used, but it is found that an important characteristic of boundary-value problems, namely that the influence of boundary conditions extends upstream, is nevertheless retained. The details of this upstream influence depend on the imposed boundary conditions. No-slip (wall) type and symmetry (wake) type boundary conditions produce distinctive differences in behavior.

Baum,[1] Tyson,[2] and Garvine[3] demonstrated the character of solutions along a body surface using finite-difference methods. It was found that if initial conditions are chosen to be consistent with ordinary boundary-layer development, the subsequent solution becomes extremely sensitive to small perturbations in these initial profiles. Two types of divergent behavior occur about a singular envelope solution which represents the usual boundary-layer solution with viscous-inviscid flow interaction effects accounted for. An example of pressure distributions for the envelope solution and the two types of divergent solutions are shown in Fig. 1 on the rounded shoulder of a body prior to separation. In one case, the pressure drops rapidly below that of the envelope solution. In other case, the pressure rises above that of the envelope solution with a corresponding decrease in

Presented as Paper 70-792 at the AIAA 3rd Fluid and Plasma Dynamics Conference, Los Angeles, Calif., June 29–July 1, 1970; submitted July 13, 1970; revision received January 14, 1972. This work was supported by the Advanced Research Projects Agency of the Department of Defense, and administered by the Space and Missile Systems Organization of the Air Force Systems Command, Norton Air Force Base, San Bernardino, Calif. under Contract F04701-70-C-0152. The authors wish to express their appreciation to M. A. Bilyk for his expert programing of the method outlined in the present paper, and to K. J. Touryan and P. J. Roache at the Sandia Corp. for their invaluable computing support.

Index category: Jets, Wakes, and Viscid-Inviscid Flow Interactions.

* Staff Engineer, Fluid Mechanics Laboratory. Member AIAA.

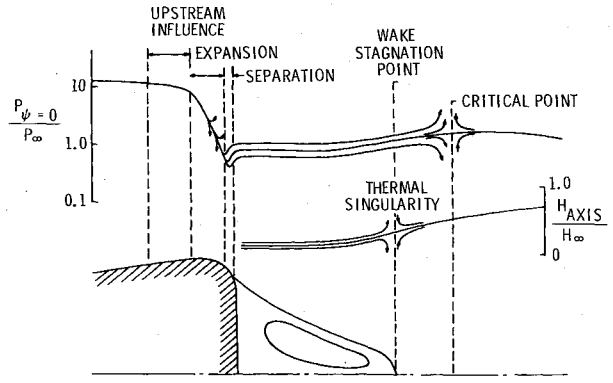

Fig. 1 Qualitative behavior of the near wake solutions.

wall shear, resulting eventually in separation. The latter solutions are of interest in the near-wake problem, since they provide a means of calculating the flow approaching boundary-layer separation on the rounded shoulder of the vehicle. It has been found that all solutions yielding separation at a given point are essentially indistinguishable, regardless of the nature of the initial perturbation. Consequently, each separation point location characterizes a single distinct upstream solution. The proper one, of the infinitude of possible separation point locations, is determined by downstream flow conditions.

The proper separation point location is resolved when the character of the solutions downstream of the wake stagnation point is examined. Depending on the initial conditions, these solutions exhibit two types of behavior, neither of which is wake-like. One family of solutions is characterized by a centerline velocity which reaches a peak downstream of the wake stagnation point, then decreases until a second stagnation point is reached (the source solutions). The other is characterized by a rapidly accelerating rate of pressure decrease on the centerline, with the calculation terminating as the rate approaches infinity (the sink solutions). This behavior is due to the presence of a saddle point singularity in the wake neck region, and is depicted by the axis pressure distributions in the wake of the body shown in Fig. 1. The singular solution which passes through the saddle point bounds the two nonwake families, and produces the only wake-like solution, where both the velocity and pressure on the centerline continue to increase downstream of the wake stagnation point. The role of this "wake critical point" in determining a unique base flow solution in a steady-state formulation has been thoroughly studied by a number of investigators, starting with Crocco and Lees.[4-10] In the present problem, the unique separation solution and associated base pressure correspond to the wake solution which passes through the critical point.

The approximate steady-state formulation of the near-wake problem, therefore, has the character of an eigenvalue problem. Any changes in boundary conditions in the region upstream of the wake singular point are felt both upstream and downstream through their influence on the eigenvalue (the separation point location). The upstream influence characteristic of boundary value problems is therefore retained, even though the governing equations are mathematically parabolic.

Based on the preceding principles, several near-wake flow models have been developed using integral moment methods.[6,11,12] These have been applied with moderate success to supersonic blunt body wakes where the Mach number is low, and the viscous-inviscid interaction is therefore weak. These integral methods are not, however, suited to applications where local flow details are important.

A model for the flow between the base and the wake stagnation point more directly applicable to slender body wakes was developed by Weiss.[13] However, the solution is not carried downstream through the critical point, and hence the base pressure must be specified using empirical means. The Weiss model was the first attempt to couple a recirculation region calculation based on the Navier-Stokes equations with a calculation of the adjacent shear layer and rotational inviscid flow. Difficulties in maintaining rigorous coupling between the modeled regions of the flow plus the need for time-consuming calculations of the recirculation region, especially at the higher Reynolds numbers of interest, lessens the desirability of this approach.

2. Description of the Model

The near-wake of a slender body in supersonic flow is characterized by many physical features, the first of which is the boundary-layer interaction with the outer, inviscid flow on the shoulder of the body. This includes the approach to separation and the resulting rise in pressure which leads to the formation of the lip shock wave so thoroughly studied by Hama.[14] After separation, a shear layer develops between the outer inviscid wake of the highly-expanded boundary-layer, and the inner recirculation region. The lip shock can propagate into the flow above the shear layer. A compression occurs near the wake stagnation point as the flow turns toward a parallel to the axis. The wake shock wave is thereby formed and propagates into the flow, eventually intersecting the lip shock wave. The flow above the shock waves was generally thought to be inviscid but rotational; however, measurements by Batt and Kubota[15] indicated significant viscous effects can be present at low Reynolds number.

The above general features have been included in the present model for flows behind bodies with rounded aft shoulders. The approach is to divide the flow into two regions which are, respectively, interior and exterior to a streamline which lies adjacent to the dividing streamline over the recirculation region and to the axis, downstream of the wake stagnation point. The inner region is described by an integral method in which the conservation equations are integrated from the axis to the "matching streamline" separating the two regions. The outer region is described by a finite difference method, using conservation equations which retain both the inviscid terms and boundary-layer-like viscous terms. A strict matching of essential flow properties is maintained between the two regions.

2.1 Outer Flow Description

A natural or intrinsic coordinate system formed by streamlines and normals to streamlines is used to describe the outer flow. If s and n represent distances along, and normal to, streamlines, respectively, then orthogonal independent variables ψ, S, and ϕ can be formed where $d\psi = \rho U r^\alpha dn$, $dS = ds/h_s$, and ϕ = azimuthal angle (when $\alpha = 1$). The metrics are $h_\psi = 1/(\rho U r^\alpha)$, $h_\phi = r^\alpha$, and h_s (to be determined later). This coordinate system and set of independent variables has a number of advantages in the present problem. Dropping the streamwise second derivatives yields a single set of governing equations which are applicable to both the flow on the body (including the rounded shoulder), as well as the wake flow above the dividing streamline. These equations are inclusive of the classical boundary-layer-like equations used to describe the body boundary layer, the shear layer, and the downstream viscous wake. In addition, they contain the complete inviscid formalism even in the viscous regions of the flow. They are therefore well-suited for describing the expansion of the boundary layer about the rounded shoulder, where viscous effects become important in a progressively thinner region, and for describing the origins of the lip and wake shock waves as diffuse compressions well within the viscous regions. Since the cross-stream viscous terms are included throughout, it is unnecessary to distinguish between the viscous and inviscid regions of the flow in the formulation; the inviscid regions will appear as a natural outcome of the analysis.

The Navier-Stokes and energy equations in this coordinate system are given in Ref. 16. Dropping all terms containing second derivatives with respect to S leads to the forms of the momentum and energy equations applied here:

$$\partial U/\partial S + (1/\rho U)(\partial P/\partial S) = (\partial/\partial\psi)[\mu h_s r^{2\alpha} \rho U(\partial U/\partial\psi)] \quad (1)$$

$$U(\partial\theta/\partial S) + h_s r^{\alpha}(\partial P/\partial\psi) = \tfrac{4}{3}(\partial/\partial\psi)\,[\mu h_s r^{2\alpha}\rho U^2(\partial\theta/\partial\psi) \quad (2)$$

$$\partial H/\partial S = (\partial/\partial\psi)\,[(\mu/Pr)h_s r^{2\alpha}\rho U(\partial H/\partial\psi)] + (\partial/\partial\psi) \cdot[(Pr - 1/Pr)\,\mu h_s r^{2\alpha}\rho U^2(\partial U/\partial\psi)] \quad (3)$$

By relating this coordinate system to the Cartesian system (Ref. 16), two additional relations are obtained after eliminating, by cross-differentiation, derivatives with respect to r and x; thus

$$\partial(\rho U r^{\alpha})^{-1}/\partial S = h_s(\partial\theta/\partial\psi) \quad (4)$$

$$\partial h_s/\partial\psi = -(\rho U r^{\alpha})^{-1}\,(\partial\theta/\partial S) \quad (5)$$

In addition, an ideal gas equation of state is used, and for the present application, the viscosity is assumed to vary linearly with temperature. The complete set of equations for the dependent variables θ, P, U, H, ρ, h_s is thus formed.

The relationship of this coordinate system to the Cartesian system is

$$\begin{aligned} \partial x/\partial S &= h_s\cos\theta \qquad & \partial x/\partial\psi &= -\sin\theta/\rho U r^{\alpha} \\ \partial r/\partial S &= h_s\sin\theta & \partial r/\partial\psi &= \cos\theta/\rho U r^{\alpha} \end{aligned} \quad (6)$$

Implicit finite-difference approximations are used to represent the equations, and since they are mathematically parabolic in character, they are solved by marching in the streamwise direction beginning with specified initial profiles on the body upstream of the shoulder. The boundary conditions will be discussed subsequently. Details of the differencing and of the method of solution of the difference equations can be found in Ref. 16.

The governing equations are unstable in regions of subsonic flow[8] in the same sense that the heat conduction equation is unstable when time is incremented backwards; that is, perturbations of small wavelength are amplified so that without some sort of smoothing, noise soon dominates the solution. This instability can be suppressed by replacing the ψ-momentum equation in the subsonic region by the boundary-layer approximation $\partial P/\partial\psi = 0$, or the higher-order approximation in which $\partial\theta/\partial S$ in the ψ-momentum equation is evaluated at the wall.

2.2 Inner Flow Description

An important consideration in developing an inner flow model is the matching of basic flow properties on the streamline between the inner and outer regions. The outer flow has the character of an initial value problem in the present formulation, where as the flow in the inner region has the character of a boundary value problem in a Navier-Stokes formulation. Stable finite-difference methods differ in each region (streamwise marching methods verses relaxation methods, respectively), and this makes the matching of basic flow properties between the two regions at each computing step extremely difficult and, in fact, impractical from a computing time standpoint unless the matching constraints are greatly relaxed. However, the use of integral methods to describe the inner flow is compatible with the finite-difference streamwise marching methods used in the outer region. Here, the governing partial differential equations, written in an axisymmetric or two-dimensional Cartesian coordinate system, are integrated from the axis to the matching streamline to form ordinary differential equations with the axial coordinate as the independent variable. The set of ordinary differential equations can be solved by a numerical marching integration from the base in step with the outer flow marching solution in a way which permits a rigorous matching of basic flow properties between the two regions at each computing step. Satisfying the conservation equations in an average (rather than in a numerically exact) sense, with a rigorous. (rather than a loose), matching to the outer flow is the approach chosen here.

Applying an integral method to a boundary value problem does not change the mathematical character to that of an initial value problem since the boundary conditions must also be considered. Ohrenberger[17] used an integral method to determine the flow in a Stokes flow recirculation region, and found that the boundary conditions must be applied both at the base and at the wake stagnation point. Thus, unlike that of an initial value problem, the boundary conditions spanned the entire flow domain as would be expected in a boundary value problem. This feature complicates the computing procedure in the present application since it requires that unknown initial conditions be systematically varied in a succession of integrations (in the direction of the outer flow) until the downstream boundary conditions are satisfied. However, by solving boundary layer-like equations rather than the full Navier-Stokes equations, this procedure can be simplified without significantly affecting the integral solution in the strongly-interacting regions of the flow.

The basic assumptions are that the axial normal stresses and axial heat conduction are neglected in the axial momentum and energy equations, respectively, and that the static pressure varies in the axial coordinate only. As a consequence of these assumptions, the base wall boundary layers, including base wall heat transfer, are neglected in the analysis. Calculations[18] and flight data[19] show that the lateral changes in pressure across the reinculation region decrease significantly with increasing Reynolds number. Evidently, as viscous effects diminish in importance, the inertia of the recirculatory flow is by itself too small to maintain large radial pressure gradients. The inference is that the present analysis is best applicable at high Reynolds numbers. However, even at low Reynolds numbers, the lateral pressure change across the recirculation region becomes small near the wake stagnation point, where most of the viscous-inviscid interaction is occurring because of the turning of the flow parallel to the axis.

Under the stated assumptions the integral forms of the axial momentum, energy, continuity, and velocity moment-of-momentum equation are, respectively:

$$\left(I_m - \frac{\gamma P}{\lambda\rho_\delta u_\delta^2}\right)\frac{\delta}{\gamma P}\frac{dP}{dx} + I_\theta = -\frac{\gamma-1}{\gamma}\frac{(q_r)_\delta}{Pu_\delta}(1 - I_q) - \frac{(\tau_{rx})}{\rho u_\delta^2} + \frac{\gamma-1}{\gamma}\frac{\delta}{Pu_\delta}\Phi_\delta I_\phi \quad (7)$$

$$(d/dx)\,(\rho_\delta u_\delta h_\delta \delta^\lambda I_e) = u_\delta\delta^\lambda I_u\,(dP/dx) - \delta^\alpha(q_r)_\delta + \delta^\lambda\Phi_\delta I_d \quad (8)$$

$$\psi_\delta = \rho_\delta u_\delta \delta^\lambda I_u \quad (9)$$

$$\tfrac{1}{2}(d/dx)(\rho_\delta u_\delta{}^3\delta^\lambda I_{mm}) = -u_\delta\delta^\lambda(dP/dx)I_u + u_\delta\delta^\alpha(\tau_{rx})_\delta I_\tau \quad (10)$$

Following Ref. 9, Eq. (7) is obtained by combining the momentum, energy, continuity, and state equations prior to forming the integral equation. This form clearly delineates the critical point singularity as the point where the term $I_m - \gamma P/(\lambda\rho_\delta u_\delta{}^2)$ vanishes.

The integrals appearing in these equations are (barred quantities are normalized by their corresponding values on the matching streamline):

$$I_\theta = \int_0^1 \bar\rho\bar u^2\,\partial(\eta^\alpha v/u)/\partial\eta d\eta,\quad I_m = \int_0^1 \bar\rho\bar u^2\,\eta^\alpha d\eta,\quad I_q = \int_0^1 \bar q_r\,\partial(\bar\rho\bar u)/\partial\eta\,\eta^\alpha d\eta,$$

$$I_\phi = \int_0^1 \bar\rho\bar u\ \bar\Phi\eta^\alpha d\eta,\quad I_e = \int_0^1 \bar\rho\ \bar h\ \bar u\ \eta^\alpha d\eta,\quad I_u = \int_0^1 \bar u\ \eta^\alpha d\eta,\quad I_c = \int_0^1 \bar\rho\ \bar u\ \eta^\alpha d\eta$$

$$I_{mm} = \int_0^1 \bar\rho\ \bar u^3\,\eta^\alpha d\eta,\quad I_d = \int_0^1 \bar\Phi\eta^\alpha d\eta,\ \text{and}\ I_\tau = \int_0^1 \bar\tau\ \partial\bar u/\partial\eta\,\eta^\alpha d\eta$$

These are evaluated by assuming radial profile shapes for $\bar\rho\bar u$, $\bar h$, $\bar q$, $\bar\tau$, and $\bar\Phi$ of the following power law forms:

$$\bar\rho\ \bar u = \xi + (1-\xi)\eta^\sigma \quad (11)$$

$$\bar h = \phi_1 + (1/2)[(2+\sigma)(1-\phi_1) - \phi_2]\eta^\sigma + (1/2)[\sigma(1-\phi_1) - \phi_2]\eta^{\sigma+2} \quad (12)$$

$$\bar\tau = \bar q = \eta^{\sigma-1},\quad \bar\Phi = \eta^{2(\sigma-1)} \quad (13)$$

where $\eta = r/\delta$. The corresponding streamfunction profile from which v can be determined for substitution in the I_θ integral is

$$\psi - \psi_\delta = \rho_\delta u_\delta\delta^\lambda[\xi(\eta^\lambda - 1)/\lambda + (1-\xi)(\eta^{\lambda+\sigma} - 1)/(\lambda+\sigma)] \quad (14)$$

The four profile parameters ξ, σ, ϕ_1, and ϕ_2 are dependent variables which vary with x, and it is seen that $\xi = \bar{\rho}_0\bar{u}_0$, $\phi_1 = \bar{h}_0$, and $\phi_2 = (\delta/h_\delta)(\partial h/\partial r)_\delta$.

For very large values of σ, these simple profiles can describe the flow close to the base where the shear layer is thin compared to the base height. The exponent $\sigma(x)$ is expected to decrease continually from that at the base to reflect the growth of the shear layer. However, a lower limit of 2 is imposed to insure a proper behavior of the flow in the vicinity of the wake stagnation point, and further downstream. A study of isolated stagnation point flows by Cheng[20] revealed that the streamline pattern for the wake stagnation point is one in which the dividing streamline is parabolic and normal to the axis at the stagnation point, i.e.

$$\lim_{x\to x_s} y_{DSL} \sim (x_s - x)^{1/2} \tag{15a}$$

and the following velocity relation applies:

$$\lim_{x\to x_s} \frac{u_0}{u_{DSL}} = -\frac{(1+\alpha)}{2} \tag{15b}$$

From the profile given by Eq. (11), it can be shown that

$$\rho_0 u_0/\rho_{DSL}u_{DSL} = -(1+\alpha)/\sigma \tag{16}$$

Thus, in order to approximate the condition expressed by Eq. (15b), it is desirable that $\sigma \approx 2$ at the wake stagnation point.† This is imposed by replacing the velocity moment-of-momentum equation (Eq. 10) with an exponential decay of σ to the value of 2, i.e., $d\sigma/dx \sim (\sigma - 2)$, just upstream of the wake stagnation point. When $\sigma = 2$, the profiles are consistent with a truncated analytic series expansion about the axis, and are therefore a good representation of actual profiles downstream of the wake stagnation point where the boundary streamline lies very close to the axis.

Although all of the dependent variables in the governing equations are to be calculated simultaneously in conjunction with the marching solution for the outer flow, the formulation is developed by considering some to be dependent variables of the inner region calculation, and the remainder to be provided by the outer region calculation. The latter include the shape of the matching streamline (through a specification of the flow angle $\theta(x)$ along it) and gradients associated with the shear stress (or vorticity) and heat transfer at the matching streamline $[(\partial U^2/\partial\psi)_\delta$ and $(\partial H/\partial\psi)_\delta]$. Since $\theta_\delta(x)$ is known, the shape of the matching streamline is obtained from the relation

$$\delta(x) = \int_0^x \tan\theta_\delta(x)dx + \delta(0) \tag{17}$$

The remaining inner flow dependent variables are $\rho_\delta, u_\delta, P, \xi, \sigma, \phi_1$, and ϕ_2, where the state equation (a thermally and calorically perfect gas is assumed) is used to eliminate h_δ. Three additional equations are therefore required and two are obtained by imposing conditions on the radial gradients of the assumed profiles by matching the vorticity and heat transfer with the corresponding outer flow values on the matching streamline. Consistent with the outer flow analysis, streamwise gradients are assumed small compared with cross stream gradients, and the resulting expressions are, respectively:

$$-\tfrac{1}{2}\rho_\delta\delta^\alpha\left(\frac{\partial U^2}{\partial\psi}\right)_\delta = -\frac{u_\delta}{\delta}[\sigma(1-\xi)+\phi_2] + 2\tan\theta_\delta\frac{du_\delta}{dx} + u_\delta\frac{d\tan\theta_\delta}{dx} + \frac{u_\delta}{\delta}\tan^2\theta_\delta[1-\lambda+\sigma(1-\xi)+\phi_2] + \frac{u_\delta}{\rho_\delta}\tan\theta_\delta\frac{d\rho_\delta}{dx} \tag{18}$$

$$\left(\frac{\gamma-1}{\gamma}\right)\frac{\rho_\delta^2 u_\delta\delta^\lambda}{P}\left[\left(\frac{\partial H}{\partial\psi}\right)_\delta - \tfrac{1}{2}\left(\frac{\partial U^2}{\partial\psi}\right)_\delta\right] = \phi_2 - \sin\theta_\delta\cos\theta_\delta\,\delta\left(\frac{1}{P}\frac{dP}{dx} - \frac{1}{\rho_\delta}\frac{d\rho_\delta}{dx}\right) \tag{19}$$

† Equation (15b) would be applied explicitly as a boundary condition in an integral formulation based on the full Navier-Stokes equations (see Ref. 17), and would be satisfied by performing successive integrations from the base as discussed previously. The present modeling alleviates the need for this procedure.

The shear term, $(\tau_{rx})_\delta$, appearing in Eqs. (7) and (10), can be written as $(\tau_{rx})_\delta/u_\delta = 2(\partial u/\partial r)_\delta + \zeta_\delta$; the first term is evaluated from the profiles and the second term, ζ_δ (the vorticity), from the outer flow. Thus,

$$(\tau_{rx})_\delta/\mu_\delta = 2\frac{u_\delta}{\delta}[\sigma(1-\xi)+\phi_2] - \tfrac{1}{2}\rho_\delta\delta^\alpha\left(\frac{\partial U^2}{\partial\psi}\right)_\delta \tag{20}$$

So that all of the heat transfer crossing the matching streamline is accounted for in the overall energy equation [Eq. (8)], $(q_r)_\delta$ is evaluated from the outer flow and is

$$(q_r)_\delta = -\frac{\mu_\delta\rho_\delta u_\delta\delta^\alpha}{Pr}\left[\left(\frac{\partial H}{\partial\psi}\right)_\delta - \tfrac{1}{2}\left(\frac{\partial U^2}{\partial\psi}\right)_\delta\right] \tag{21}$$

The dissipation term, Φ_δ, appearing in Eqs. (7) and (8), is also evaluated from the outer flow, and consistent with the outer flow approximations is

$$\Phi_\delta = \mu_\delta\left[\tfrac{1}{2}\rho_\delta\delta^\alpha\left(\frac{\partial U^2}{\partial\psi}\right)_\delta\right]^2 \tag{22}$$

A centerline equation was chosen as the final governing relation in order to provide some balance to the conditions imposed on the profiles at the matching streamline. At first, it seemed desirable to use both the centerline momentum and energy equations, in lieu of the moment-of-momentum equation [Eq. (10)]. However, $(\partial P/\partial x)_o$ appears in each equation and is unknown on the axis. The quantity dP/dx calculated in the analysis is a weighted pressure gradient influenced primarily by the high momentum outer low. Applying it to the relatively low momentum centerline flow near the base, where $\partial P/\partial r$ can be significant, leads to completely erroneous results. For this reason, the centerline momentum and energy equations were combined to eliminate $(\partial P/\partial x)_o$, and a single centerline equation for the axis total enthalpy was the result:

$$\rho_o u_o\frac{dH_o}{dx} = \lim_{r\to 0}\frac{\mu}{r^\alpha}\left[\frac{\partial}{\partial r}\left(\frac{\partial u}{\partial r}\right) + \frac{1}{Pr}\frac{\partial}{\partial r}\left(\frac{\partial h}{\partial r}\right)\right] \tag{23}$$

The right hand side of Eq. (23) is evaluated from an analytic expansion of the profiles about the axis, with the coefficients of the quadratic terms evaluated by joining with the power law profiles at some arbitrary value of η (denoted as η^*). The profiles are thus approximated by

$$\bar{\rho}\;\bar{u} = \xi + (1-\xi)\eta_*^{\sigma-2}\eta^2,\quad \bar{h} = \phi_1 + \phi_1\eta_*^{\sigma-2}\eta^2 \tag{24}$$

where

$$\Phi_1 = \tfrac{1}{2}[(2+\sigma)(1-\phi_1) - \phi_2]$$

Eq. (23) can then be written as

$$\rho_\delta u_\delta\xi\frac{d}{dx}\left[\tfrac{1}{2}(\phi_1 u_\delta\xi)^2 + \frac{\gamma}{\gamma-1}\frac{\phi_1 P}{\rho_\delta}\right] = \frac{2\lambda_1\mu_o}{\delta^2}\left\{\xi u_\delta^2\phi_1[\phi_1(1-\xi)+\xi\phi_1] + \frac{1}{Pr}\frac{\gamma}{\gamma-1}\frac{P}{\rho_\delta}\phi_1\right\}\eta_*^{\sigma-2} \tag{25}$$

where the state relation is used to eliminate h_δ. The value chosen for η_* affects the results only slightly since the right hand side of Eq. (25) becomes important only near the wake stagnation point where δ is small and $\sigma \approx 2$.

Near the base, where the shear layer is thin compared with δ, both δ and σ are large. The right hand side of Eq. (25) is therefore very small, and the axis flow is essentially adiabatic at a constant value of H_o. Near the wake stagnation point, the centerline flow does shear work and loses heat to [R.H.S. of Eq. (23)] the adjacent flow moving toward the wake stagnation point. The axis total enthalpy thus diminishes away from the wake stagnation point and reaches a plateau value as the radial extent of the recirculation region—i.e., δ increases. The plateau value is thus dictated by the history of the flow proceeding toward the base, and is therefore unknown a priori. However, since the governing equations are numerically integrated from the base, the plateau value of H_o is required initially. This apparent

conflict is resolved by the presence of a singularity at the wake stagnation point, which is evident by inspection of Eq. (25) when $\xi = 0$.

It can be shown that the solution of Eq. (25) near the wake stagnation point is given by

$$h_o(x) = h_{\delta s}(1 - \tfrac{1}{4}\phi_{2s}) - \tfrac{1}{4}C(x_s - x)^{-\varepsilon} \tag{26}$$

where

$$\varepsilon = 4\lambda\, \mu_{os}/Pr\, \delta_s^2(d\rho_o u_o/dx)_s > 0$$

The constant of integration, C, is adjusted to permit a matching of the above solution to the numerical solution from the base. Clearly, h_o becomes very large or small depending on the sign of C, and only when $C = 0$ is h_0 well behaved. The initial value of h_0 can be treated as an eigenvalue and varied systematically in a succession of integrations until the condition that $C = 0$ is closely bracketed. Equation (26) with $C = 0$ can then be used to jump across the singularity, or the integration can be carried through the singularity, since the recovery of the divergent solution also occurs exponentially, and for some cases it has been found that the perturbation on the outer flow solution is negligible. The character of this singularity is illustrated in Fig. 1.

The "thermal" singularity may be interpreted as a heat source or sink which is present to accommodate the requirement that the net heat flux across the dividing streamline must be equivalent to the heat generated by viscous dissipation in the recirculation region (minus the heat transferred to the base if base heat transfer were included). The net heat transfer is affected by the axis enthalpy, the level of which is strongly influenced by the assumed initial value. The proper initial value produces the desired nondiverging balance between dissipation and heat transfer.

This completes the description of the inner flow analysis. In summary, eight equations [Eqs. (7, 8, 9, 10, 17, 18, 19, and 25)] are solved simultaneously using a Runge-Kutta second order method for eight unknowns (δ, u_δ, ρ_δ, P, ξ, σ, ϕ_1, and ϕ_2) with $\theta_\delta(x)$, $(\partial U^2/\partial\psi)_\delta$, and $(\partial H/\partial\psi)$ given along the matching streamline. The initial values of δ, u_δ, ρ_δ, P, and ϕ_2 are known from the separation solution on the chosen matching streamline. Since h_o is unknown, initial values of ϕ_1 $(= h_o/h_\delta)$ are assumed until two solutions (and hence two values of h_o) are found which closely bracket the singularity at the wake stagnation point. The initial value of ξ is zero to reflect the presence of the base wall. The initial σ is determined from continuity, Eq. (9), knowing the mass flux, ψ_δ, associated with the matching streamline. The solution is obtained in a step-by-step calculation in conjunction with the marching solution for the outer flow; the details of the coupling scheme are described in the next section.

3. Boundary and Initial Conditions

Boundary conditions for the outer region must be specified initially, on the outer streamline boundary, and on the wall or inner matching streamline.

The initial profiles of U, H, P, θ, and h_s are determined along a normal, to-the-body surface well upstream of the body shoulder from a solution to the boundary-layer equations. The outer boundary of the calculation for both the attached flow on the body shoulder and the wake region is a streamline which lies initially somewhat outside the body boundary-layer but within the shock layer. Diffusive effects are assumed negligible along this streamline, and the coupling with the outer inviscid flow is represented by the differential form of the Prandtl-Meyer relation. Any errors introduced by this simplified description of the outer flow propagate inwards toward the viscous layer along a right-running characteristic. The inner region bounded by this characteristic is unaffected by the boundary condition if it is a true characteristic (that is, if diffusive effects are locally negligible). This representation of the boundary conditions can therefore be used for axisymmetric or initially rotational (but inviscid) flows simply by including a large enough domain in the initial conditions so that the region of interest always lies within the region of influence of the initial line.

The standard no slip and enthalpy-specified boundary conditions are imposed on the body shoulder for the attached flow approaching separation.

Downstream of the separation point P, U^2, H, $\partial U^2/\partial\psi$, $\partial H/\partial\psi$ and θ are matched at the boundary between inner and outer regions. Matching is achieved by iteration, initiated by estimating the values of $\partial U^2/\partial\psi$, $\partial H/\partial\psi$ and θ at the end of the streamwise step. Using these input values, the inner region calculation provides corresponding values of P, U^2 and H and in addition numerically determines the nine partial derivatives of P, U^2 and H with respect to $\partial U^2/\partial\psi$, $\partial H/\partial\psi$ and θ. Taylor's series expansions, retaining only linear terms, then are used to generate linear relations $P(\partial U^2/\partial\psi, \partial H/\partial\psi, \theta)$ etc., valid in the neighborhood of the initial estimated values. These linear relations are used as boundary conditions for the outer region calculation, which produces new values of $\partial U^2/\partial\psi$, $\partial H/\partial\psi$ and θ. The iterations are continued until all six variables agree between inner and outer regions and between succeeding iterations within a specified tolerance.

4. Method of Solution

The first step in obtaining a near-wake solution is the generation of a series of separation solutions corresponding to different separation points, and hence separation pressures, on the curved body shoulder. As pointed out in the introduction, diverging solutions are required to describe separation and can be generated by systematically perturbing the initial profiles. However, a great deal of computing time would be saved if a method were available to selectively obtain the envelope solution from which the diverging solutions could be initiated on the rounded shoulder. Such a method was suggested by H. K. Cheng (private communication) who noted that the divergent solutions are rejected if $\partial P/\partial S$ in the streamwise momentum equation in the subsonic region of the flow is evaluated at the preceeding S-step. The envelope solution can thus be generated directly, and the separation solutions are then initiated from the envelope solution by re-introducing the consistent evaluation of $\partial P/\partial S$. If the resulting divergent solution is not of the separation family, an infinitesimal perturbation of the velocity profile is used to induce separation on a succeeding calculation.

The wake solution is initiated from the terminal step (which lies along a normal to streamlines originating on the body surface just upstream of the actual separation point) of a chosen separation solution. An initial coupling point, and hence matching streamline, are chosen below the root of the lip shock from which initial conditions on the dependent variables for the inner region are obtained. A value for the initial axis enthalpy is assumed, and a coupled inner and outer solution is generated by marching downstream. Its behavior near the thermal singularity and approaching the critical point singularity determines whether the chosen separation pressure (corresponding to the separation solution) and initial axis enthalpy are larger or smaller than the sought-after singular values. The process is repeated with new separation solutions and initial axis enthalpies until the singular values are bracketed to the desired degree.

5. Comparison of Theory with Experiment

A series of experiments were conducted by Batt[21] for the purpose of measuring flow properties in the laminar near wake of a 10° half-angle wedge at $M_\infty = 6$ for both adiabatic and cold wall surface conditions. Pitot pressure, total temperature, mass flux, and axis static pressure were measured, and since they represent a complete self-consistent set of data, a number of other flow properties (velocity, static pressure, static temperature, total pressure, Mach number) can be determined. Profiles at several axial stations in the near wake, as well as flow-field mappings, were presented for four Reynolds numbers, spanning the range $1.4 \times 10^4 < Re_{\infty H} < 5.5 \times 10^4$. The choice of the case with which the theory is compared was predicated on several factors. First, a cold wall body was felt to be a more

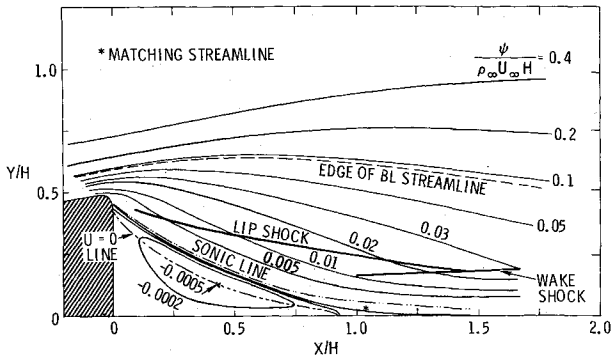

Fig. 2 Streamline map ($Re_{\infty H} = 4.1 \times 10^4$, $M_\infty = 6$, $T_w/T_{o\infty} = 0.19$, 10° half-angle wedge): near wake theory.

difficult case and would therefore constitute a better test of the theory. Second, the experiments were performed on models with a sharp-cornered base, whereas the theory requires a rounded shoulder with a minimum corner radius related to the thickness of the subsonic portion of the boundary-layer. The closest theoretical simulation would therefore correspond to the highest Reynolds number cold wall experiment. However, this case was excluded because of possible transition effects. Thus, the cold wall ($T_w/T_{o\infty} = 0.19$) second highest Reynolds number ($Re_{\infty H} = 4.1 \times 10^4$) experiment was chosen for the comparisons with a corner radius of $0.05H$ used in the calculation.

The determination of initial boundary-layer profiles for use in the calculations presents some problems, since measurements were not made upstream of the corner. However, the measured streamfunction profile in the inviscid shock layer at the corner could be used to obtain a displacement thickness, and a Blasius boundary layer with $\mu \sim T$ and $Pr = 1$ which matched the measured displacement thickness was used. The resulting thickness was found to be 68% larger than that for a similar noninteracting boundary layer on a sharp wedge. This disturbingly large difference may be due mostly to the thickening effect of the relatively hot solid leading edge of the otherwise cryogenically cooled model, and to the nonsimilar boundary layer development thereafter.

The separation pressure and the initial centerline temperature in the recirculation region were bracketed within the following tolerances:

$$P/P_\infty = 0.2399 \pm 0.0004,\ T/T_{o\infty} = 0.203 \pm .001$$

The experimental axis pressure is $P/P_\infty = 0.218$ ($\pm$ .004) at the base. The axis temperature in the recirculation region was not measured.

A flowfield map from the calculation is shown in Fig. 2 and can be compared to that presented by Batt and Kubota.[15] The most striking difference is that the experimental separation-point location lies lower on the base than calculated here. This results in a high theoretical lip shock location (by about $0.04H$), and probably a high dividing streamline location, since the wake stagnation point is displaced downstream from the measured location ($x_s/H = 0.93$ as compared with $[x_s/H]_{exp} = 0.75$). Since these details are strongly dependent on the local flow behavior near the body shoulder, which differs geometrically between theory and experiment, this discrepancy is hardly surprising. Features expected to be less sensitive to shoulder geometry agree quite well, including the wake shock position and the locations of the streamlines. Figure 2 presents several features of the flow not measured by Batt, including the dividing streamline shape (note the significant curvature), and the center of the vortex. The streamfunction (-0.0005) associated with the vortex center was found to be extremely small compared with that defining the outer edge of the interacting region of the near wake (0.01–0.02), which may explain why even small rates of gas injection into the recirculation region from the base wall can significantly affect experimental results in two-dimensional separated flows.[22]

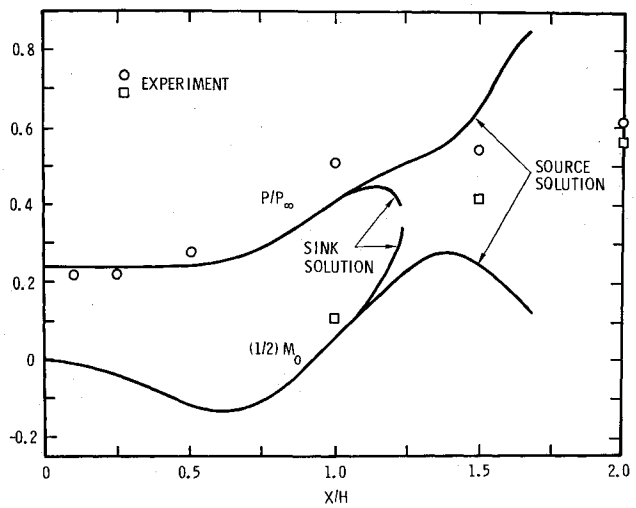

Fig. 3 Wake centerline static pressure and Mach Number: comparison with measurements of Batt ($Re_{\infty H} = 4.1 \times 10^4$, $M_\infty = 6$, $T_w/T_{o\infty} = 0.19$, 10° half-angle wedge).

Axis pressure and axis Mach number distributions for the two solutions of opposite families which bracket the critical point are shown in Fig. 3. The calculated pressure rise due to the turning of the flow near the wake stagnation point is displaced slightly downstream of the measurements. This is consistent with the observations in Fig. 2 that the calculated location of the wake stagnation point is also downstream from the measured location. The results in the ensuing figures at $x/H = 1.5$ are taken from the source solution.

Calculated pitot pressure profiles (normalized by the freestream total pressure) are compared with direct measurements in Fig. 4 at five axial stations spanning the near wake. The lip shock is evident from the S-shaped break in the pitot profiles at $x/H = 0.1$, 0.25, 0.50 and at $x/H = 1.0$, where both the lip and wake shocks are present. A single merged shock exists at $x/H = 1.5$. The calculated and measured shock strengths based on the change in pitot pressure appear to be in reasonable agreement at the respective stations. However, the calculated lip shock lies slightly above the measured location, as discussed previously.

In Fig. 5, the calculated and measured total temperature profiles differ significantly below the inviscid region at $x/H = 0.1$. This suggests strongly that the boundary layer approaching the shoulder of the model is actually hotter than would be predicted assuming similarity. This is not a Prandtl number effect, since a comparison between $Pr = 1$ and $Pr = 0.7$ similar enthalpy profiles shows a difference much smaller than that observed in Fig. 5. This difference is most likely due, as previously noted, to residual nonsimilar effects of a hot-wall leading edge region.

Static pressure profiles from the present theory are presented in Fig. 6. Beginning at large Y/H, each profile is characterized by a sharp pressure drop as a result of the corner expansion, followed by an increase across the shock(s) to a value which remains constant to the axis. As x/H increases, the lip shock grows in strength with the pressure decreasing on the upstream side while remaining essentially constant on the downstream side.

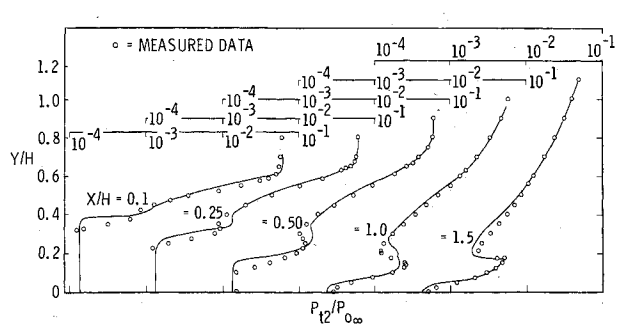

Fig. 4 Pitot pressure: comparison with measurements of Batt (Re_∞ = 4.1×10^4, $M_\infty = 6$, $T_w/T_{o\infty} = 0.19$, 10° half-angle wedge).

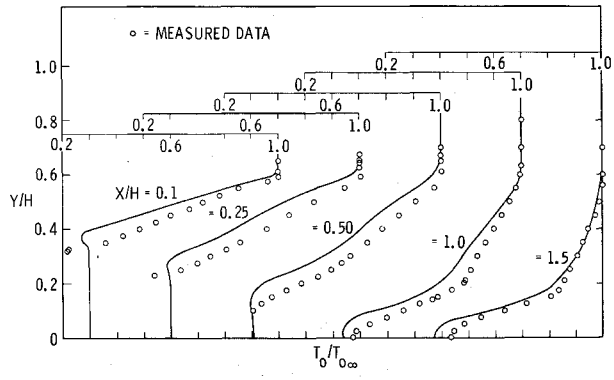

Fig. 5 Total temperature: comparison with measurements of Batt ($Re_{\infty H} = 4.1 \times 10^4$, $M_\infty = 6$, $T_w/T_{0\infty} = 0.19$, 10° half-angle wedge).

At $x/H = 1.0$, compression waves are evident below the lip shock because of the interaction which causes the flow to turn in the downstream direction in the vicinity of the wake stagnation point. A strong coalescing of both sets of compression waves occurs, producing a sharp distinct shock at $x/H = 1.5$.

The horizontal tick marks in Fig. 6 and the subsequent figures represent the edge of the initially inviscid region where the total temperature is constant. Experimental data points from Batt were calculated in this region from measurements of P_{t2} and T_0, and an approximate total pressure obtained by projecting the streamlines to the bow shock, and calculating the P_0 change across the shock based on the observed shock angle; the total pressure was then assumed constant on the streamline. The predicted static pressure is in excellent agreement with those data points calculated in this fashion. Mass flux probe data were used, together with P_{t2} and T_o, to obtain data points above the shocks in the variable T_0 region. These data points tend to be more irregular because of slight inaccuracies in curve fairing of scattered data necessary in regions of sharp flow gradients.[23]

Even so, the theoretical pressures are consistently smaller than the measurements, although the qualitative trends are in agreement. Batt[23] found that the derivation of the pressure and temperature in this region was particularly sensitive to small changes in the measured quantities. The magnitude of the total temperature discrepancy (Fig. 5) is in fact large enough to account for a large fraction of the disagreement observed in Fig. 6.

Total velocity profiles from the present theory are compared in Fig. 7 to values derived from measured data. The agreement is excellent above the lip and wake shock waves where the original low-momentum, boundary-layer fluid is accelerated by the expansion to a nearly uniform value at $x/H = 1.5$. Batt calculated the velocities below the shock using the measurements of P_{t2} and T_0 and assuming that the static pressure equals the measured axis static pressure at that axial station. Velocities calculated by the theoretical model are less than those from the experiment

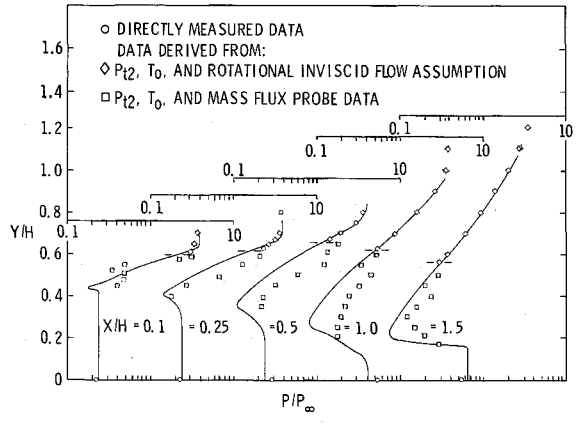

Fig. 6 Static pressure: comparison with measurements of Batt ($Re_{\infty H} = 4.1 \times 10^4$, $M_\infty = 6$, $T_w/T_{0\infty} = 0.19$, 10° half-angle wedge).

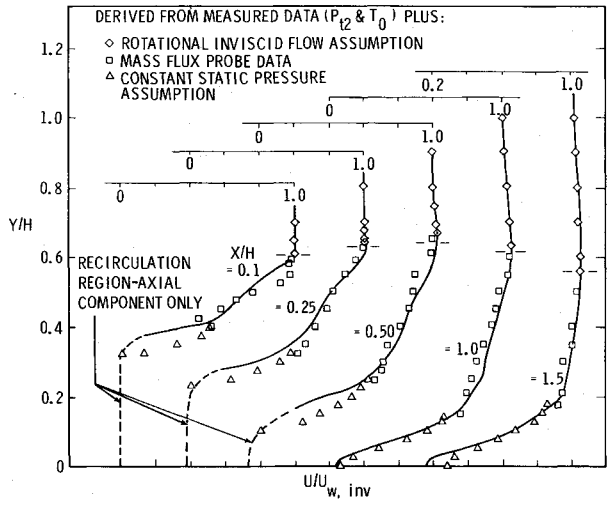

Fig. 7 Total velocity: comparison with measurements of Batt ($Re_{\infty H} = 4.1 \times 10^4$, $M_\infty = 6$, $T_w/T_{0\infty} = 0.19$, 10° half-angle wedge).

adjacent to the recirculation region; however, good agreement is maintained downstream of the wake stagnation point where large lateral gradients are in evidence.

The calculation shows that large temperature gradients in the hot core of the boundary layer are essentially eliminated as the boundary-layer fluid is cooled by the expansion. Large lateral temperature gradients are evident in the shear layer due to the mixing of hot, nearly constant temperature, recirculation region fluid with relatively cold boundary-layer fluid from near the wall. The profiles downstream of the wake stagnation point show a significant increase in temperature from the shock to the axis. Temperature profiles are presented in Ref. 16, and comparisons with the experimental data are made. Excellent agreement is maintained in the constant T_0 region (above the edge of boundary-layer streamline). However, the temperatures calculated from the measured data in the wake of the boundary-layer (using mass flux probe data) are larger than the predictions. This disagreement was traced to the discrepancies in total temperature shown in Fig. 5, and to a lesser extent to the measurements.

These comparisons suggest that the present model includes all of the qualitative features of the measured flowfield at this Reynolds number, and that rather good over-all agreement was maintained in the detailed comparisons. This is particularly true downstream of the wake stagnation point where calculations are initiated for the far wake. The discrepancies which did occur appear to be the results of the rounded shoulder required by the theoretical model; inaccuracies in the assumed total-temperature distribution in the boundary layer prior to separation, and, in part, to uncertainties in the derived experimental data.

6. Other Solutions

High Mach number ($M_\infty = 21$) ideal gas, near-wake flows for slender (8° half-angle) cones have been obtained with the present model over a wide range of Reynolds numbers, and the results are presented in Ref. 16 (space does not permit presentation here). Generally, the qualitative trends observed from these solutions are consistent with available experimental data for similar conditions.

7. Conclusions

A theoretical model of the near wake of supersonic bodies has been developed which is capable of describing not only gross effects, but local flow details as well. The analysis is self-contained downstream of the undisturbed boundary layer on the body; the separation point and base pressure are determined uniquely. The model includes viscous effects everywhere to ob-

viate the problem of defining a viscous region boundary. The effects of upstream influence on the boundary layer approaching the body shoulder are accounted for, and the approach to boundary-layer separation on a smooth, rounded body shoulder is described in detail. After separation, the continuing expansion of the wake of the boundary layer, the development of the lip and wake shock waves, the growth of the shear layer, and the flow in the recirculation region are all determined in the course of the calculation. Two-dimensional or axisymmetric bodies can be described with either an insulated or cold wall.

Comparisons with the Mach 6 cold wall wedge experiments of Batt indicate that the model includes all of the qualitative features of the measured flowfield, with a good over-all agreement in local flow details. This is particularly true downstream of the wake stagnation point where far-wake calculations are initiated.

References

[1] Baum, E., "An Interaction Model of a Supersonic Laminar Boundary Layer on Sharp and Rounded Backward Facing Steps," *AIAA Journal*, Vol. 6, No. 3, March 1968, pp. 440–447.

[2] Tyson, T. J., "Laminar Boundary Layers in the Neighborhood of Abrupt Spatial Disturbances," Ph. D. dissertation, June 1967, California Inst. of Technology, Pasadena, Calif.

[3] Garvine, R. W., "Upstream Influence in Viscous Interaction Problems," *The Physics of Fluids*, Vol. 11, No. 7, July 1968, pp. 1413–1423.

[4] Crocco, L. and Lees, L., "A Mixing Theory for the Interaction Between Dissipative Flows and Nearly Isentropic Streams," *Journal of the Aeronautical Sciences*, Vol. 19, No. 10, Oct. 1952, pp. 649–676.

[5] Webb, W. H., Golik, R. J., Vogenitz, F. W. and Lees, L., "A Multimoment Integral Theory for the Laminar Supersonic Near Wake," *Proceedings of the 1965 Heat Transfer and Fluid Mechanics Institute*, Stanford University Press, Stanford, Calif., 1965.

[6] Reeves, B. L. and Lees, L., "Theory of Laminar Near Wake of Blunt Bodies in Hypersonic Flow," *AIAA Journal*, Vol. 3, No. 11, Nov. 1965, pp. 2061–2074.

[7] Ai, D. K. Y., "On the Hypersonic Laminar Near Wake Critical Point of the Crocco-Lees Mixing Theory," AIAA Paper 67-60, New York, 1967.

[8] Baum, E. and Denison, M. R., "Interacting Supersonic Laminar Wake Calculations by a Finite Difference Method," *AIAA Journal*, Vol. 5, No. 7, July 1967, pp. 1224–1230.

[9] Weinbaum, S. and Garvine, R. W., "On the Two-Dimensional Viscous Counterpart of the One-Dimensional Sonic Throat," *Journal of Fluid Mechanics*, Vol. 39, Oct. 1969, pp. 57–86.

[10] Holt, M. and Meng, J. C. S., "The Calculation of Base Flow and Near Wake Properties by the Method of Integral Relations," *19th Congress of the International Astronautical Federation*, Paper RE65, Oct. 1968, New York.

[11] Reeves, B. L. and Buss, H., "A Theoretical Model of Laminar Hypersonic Near Wakes Behind Blunt-based Slender Bodies," AIAA Paper 68-696, Los Angeles, Calif., 1968.

[12] Grange, J., Klineberg, J. M. and Lees, L., "Laminar Boundary-Layer Separation and Near-Wake Flow for a Smooth Blunt Body at Supersonic and Hypersonic Speeds," *AIAA Journal*, Vol. 5, No. 6, June 1967, pp. 1089–1096.

[13] Weiss, R. F., "A New Theoretical Solution of the Laminar, Hypersonic Near Wake," *AIAA Journal*, Vol. 5, No. 12, Dec. 1967, pp. 2142–2149.

[14] Hama, F. R., "Experimental Studies on the Lip Shock, *AIAA Journal*, Vol. 6, No. 2, Feb. 1968, pp. 212–219.

[15] Batt, R. G. and Kubota, T., "Experimental Investigation of Laminar Near Wakes Behind 20° Wedges at $M_\infty = 6$," *AIAA Journal*, Vol. 6, No. 11, Nov. 1968, pp. 2077–2083.

[16] Ohrenberger, J. T. and Baum, E., "A Theoretical Model of the Near Wake of a Slender Body in Supersonic Flow," AIAA Paper 70-792, Los Angeles, Calif., 1970.

[17] Ohrenberger, J. T., "An Integral Formulation of the Wake Recirculation Region," 12291-6013-R0-000, Oct. 1969, TRW Systems Group, Redondo Beach, Calif.

[18] Reeves, B. L. and Buss, H., "On the Flow in Regions of Laminar Separation," AIAA Paper 67-64, New York, 1967.

[19] Cassanto, J. M., "Radial Base-Pressure Gradients in Laminar Flow," *AIAA Journal*, Vol. 5, No. 12, Dec. 1967, pp. 2278–2279.

[20] Cheng, S. I., "Flow Around an Isolated Stagnation Point in the Near Wake," RAD RM-63-23, July 1963, Avco Corp., Wilmington, Mass.

[21] Batt, R. G., "Experimental Investigation of Wakes Behind Two-Dimensional Slender Bodies at Mach Number Six," Ph. D. thesis, 1967, California Inst. of Technology, Pasadena, Calif.

[22] Chapkis, R. L. et al., "An Experimental Investigation of Base Mass Injection on the Laminar Wake Behind a 6-Degree Half-Angle Wedge at $M = 4.0$," AGARD Conference Proceedings No. 19, Fluid Physics of Hypersonic Wakes, Fort Collins, Colo., May 1967.

[23] Batt, R. G., private communication, June 1970, TRW Systems Group, Redondo Beach, Calif.